

Updated directions of IceCube HESE events with the latest ice model using DirectFit

The IceCube Collaboration

(a complete list of authors can be found at the end of the proceedings)

E-mail: tyuan@icecube.wisc.edu, dima@icecube.wisc.edu

The initial evidence of astrophysical neutrinos by the IceCube Neutrino Observatory stemmed from the high-energy starting events (HESE) sample: a selection of the highest-energy neutrino interactions that occurred within the detector fiducial volume. Each event was reconstructed based on our best knowledge of the ice at the time, with the latest results published in a description of the sample using 7.5 years of data. Since then, several major improvements in ice modeling have occurred using in-situ calibration data. These include a microscopic description of ice anisotropy arising from ice crystal birefringence and a more complete mapping of the ice layer undulations across the detector. The improvements feed into more accurate descriptions of individual events, and can especially affect the directional reconstruction of particle showers. Here, we apply the latest ice model in an exact manner to reconstruct IceCube's high-energy events using DirectFit. This reconstruction samples posterior distributions across parameters of interest by performing full event resimulation and photon propagation at each step. We obtain improved per-event descriptions, as well as updates on previously published source searches using the aggregated sample.

Corresponding authors: Tianlu Yuan^{1*}, Dmitry Chirkin¹

¹ *Dept. of Physics and Wisconsin IceCube Particle Astrophysics Center, University of Wisconsin–Madison*

* Presenter

The 38th International Cosmic Ray Conference (ICRC2023)
26 July – 3 August, 2023
Nagoya, Japan



1. Introduction

Over a decade ago the IceCube Neutrino Observatory detected the first PeV neutrinos [1], a crucial piece in the first evidence of high-energy extraterrestrial neutrinos [2]. The analysis was performed with the high-energy starting events (HESE) selection, which utilized a simple outer-layer veto coupled with a lower bound on the total detected charge of 6000 photoelectrons in order to suppress atmospheric backgrounds and select high-energy neutrino interactions within a fiducial volume. In the time since, IceCube has continued to collect data nearly without interruption. Iterative updates to the HESE sample were performed as events accumulated [3, 4]. As understanding of the ice and detector evolved, the HESE sample was reanalyzed with an increased sample size and improved models and methods [5]. Included were per-event reconstructed quantities, which for the spatial clustering analyses relied on a fully resimulated event reconstruction [6] (DirectFit¹) using an ice model that was current at the time.

Here, we provide an updated neutrino source search using the HESE sample with an extra 4.5 years of data since [5]. In addition to the increased livetime, major updates to modeling of ice anisotropy [7] and ice layer undulations [8] are taken into account. Per-event directional probability density functions (PDF) are again parameterized with the 8-parameter Fisher-Bingham (FB8) distribution to capture generalized, asymmetric PDFs on the sphere [9, 10]. The parameterized description of all events and pre-computed full-sky FITS files of their PDFs are available at [11].

2. Data sample and event reconstruction

In total, 64 new events passed the HESE selection. Events 128 and 132 contain coincident atmospheric backgrounds and are removed from the analysis. The remainder is combined with the 102 previously reported events [5] for a total of 164 events.

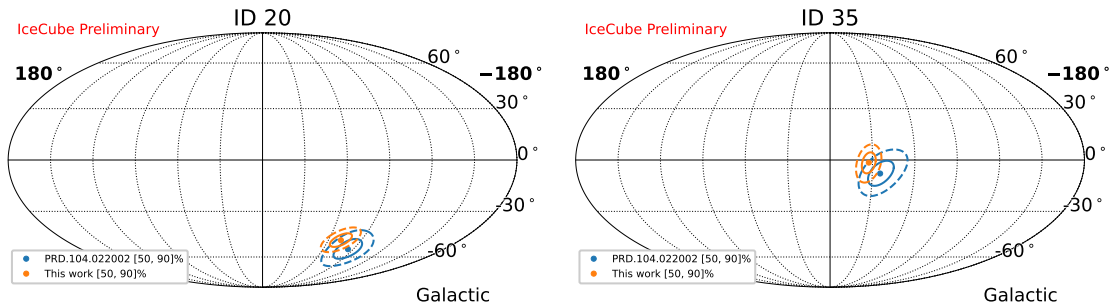


Figure 1: Comparison of the reconstructed directions and 50% (solid) and 90% (dashed) highest posterior density regions for events 20 (left panel) and 35 (right panel).

A primary goal of this proceeding is to provide per-event reconstructed quantities, including the direction and its uncertainties as well as the visible energy, using the most up-to-date ice model. This is currently only possible with DirectFit, which resimulates events as it searches through the physics parameter space and fully propagates photons on graphics processing units (GPU) through an ice model in all its descriptive detail. Its accuracy comes at a significant cost

¹Code available at <https://github.com/icecube/ppc/>

of computational complexity; for the energy ranges of HESE events and the settings used here a complete reconstruction can take on the order of hours to a day on a NVIDIA A100 GPU. Reconstructing large scale Monte Carlo (MC) datasets with DirectFit is currently not feasible. Therefore, as remarked in [5], the results presented here are not meant to be employed in a fully consistent, forward-folding likelihood fit for MC-based spectral analyses. Alternative IceCube reconstructions that apply approximations are generally faster and more applicable to spectral fits [12–14].

DirectFit was run for all 164 events, first with a localized random search routine to refine the physics parameter space over the event position and its arrival direction. This is followed by a second Approximate Bayesian Computation (ABC) routine to sample the posterior density [6]. Finally, the distribution of samples is marginalized over position and energy, and a FB8 PDF is fitted to the sample of arrival directions. In comparison to [5], the reconstruction is updated to have increased simulation photon statistics used in DirectFit as well as the ice model updates discussed earlier.

For the events already present in the previous 7.5-year dataset the reconstructions provided here may be compared to those in [5] (Appendix J). Figure 1 shows the 50% and 90% highest posterior density (HPD) regions for two PeV events that were previously published (blue) [5] to those obtained in this work (orange). Differences arise from the updates to the ice optical modeling and the smaller contours result in part due to the increased simulation photon statistics.

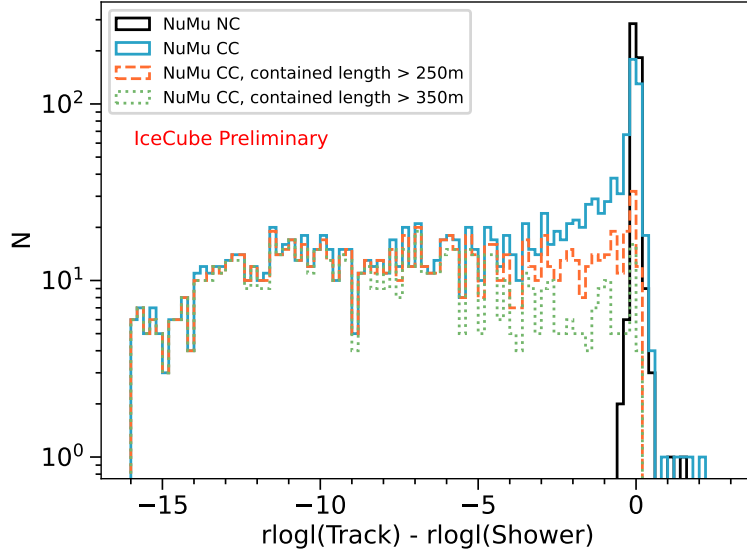


Figure 2: Distribution of the reduced negative log-likelihood difference between a track and shower reconstruction for a sample of simulated muon neutrino events. Neutral current (NC) interactions (black) produce hadronic showers and an outgoing neutrino, while charged current (CC) interactions (blue) produce an outgoing charged muon. Separability improves as the contained length increases to greater than 250 m (dashed orange) and 350 m (dotted green).

As DirectFit provides distinct algorithms for reconstruction of particle showers and high-energy muon tracks, events are first classified for the appropriate algorithm. To predetermine which

reconstruction to apply, a new classification scheme was implemented using a faster, but more approximate, reconstruction that includes recent ice model improvements [15–17]. For each event, the fast track and shower reconstruction was run to obtain the reduced negative log-likelihood (rlogl) under each hypothesis. Their difference gives the classification metric, as shown in Fig. 2 for a simulated sample of muon neutrinos. Interactions via deep inelastic scattering result in a hadronic shower and either a neutrino or a muon in the case of a neutral current (NC) or charged current (CC) interaction, respectively. More negative values correspond to more evident track signatures, and separability against showers improves for tracks with longer contained lengths inside the instrumented volume (dashed orange and dotted green). For HESE data events with $-0.8 < \text{rlogl}(\text{Track}) - \text{rlogl}(\text{Shower}) < -0.2$, a full DirectFit is then run with both track and shower reconstructions and the one yielding the best data agreement is chosen. This two step approach is taken as it is too computationally expensive to reconstruct every event with DirectFit under both shower and track hypotheses. For many events, such as in the case of an obvious track, running both routines is also unnecessary.

Event 135 is the highest-energy event in the sample. Reconstructed as a track, its most-probable visible energy is 4.8 PeV. Assuming that the track is a high-energy muon, we find $dE/dx = 1.125 \text{ TeV m}^{-1}$ in the last 400 m before exiting the detector. Sampling from a uniform initial muon energy distribution between 1 PeV to 100 PeV, and conditioning on an energy loss of 450 TeV after 400 m, the initial muon energy is found to be $(9 \pm 5) \text{ PeV}$ [18]. This corresponds to a total energy of about $(13 \pm 5) \text{ PeV}$. If the event occurred from the CC interaction of a muon neutrino, the incoming neutrino energy would be further dependent on flux assumptions and the inelasticity. Further detailed studies are ongoing.

3. Spatial clustering analysis

We performed three tests of spatial clustering, following a similar procedure as previously reported [3–5]. An unbinned, maximum likelihood function is used [19]

$$\mathcal{L}(n_s; \vec{\psi}_s) = \prod_i^N \left[\frac{n_s}{N} \cdot S(\vec{x}_i, \vec{\psi}_s) + \left(1 - \frac{n_s}{N}\right) \cdot B(\delta) \right], \quad (1)$$

where N is the total number of observed events, n_s is the expected number of signal events, $\vec{\psi}_s$ is the source position in the sky, \vec{x}_i represents the properties of event i , $B(\delta)$ is the declination-dependent background spatial distribution derived from data scrambles along a declination band δ , and $S(\vec{x}_i, \vec{\psi}_s) = P_i(\vec{\psi}_s)$ is the spatial distribution expected from the signal population which is taken to be equal to the posterior density of the event direction at the source position. For spatially extended sources, the likelihood is convolved with the spatial template over the entire sky. The TS is defined to be,

$$\text{TS} = -2 \ln[\mathcal{L}(n_s = 0) / \mathcal{L}(\hat{n}_s)], \quad (2)$$

where \hat{n}_s is best-fit value that maximizes the likelihood. The TS distribution under the null hypothesis is obtained by scrambling data in right ascension to generate pseudoexperiments expected under an isotropic flux.

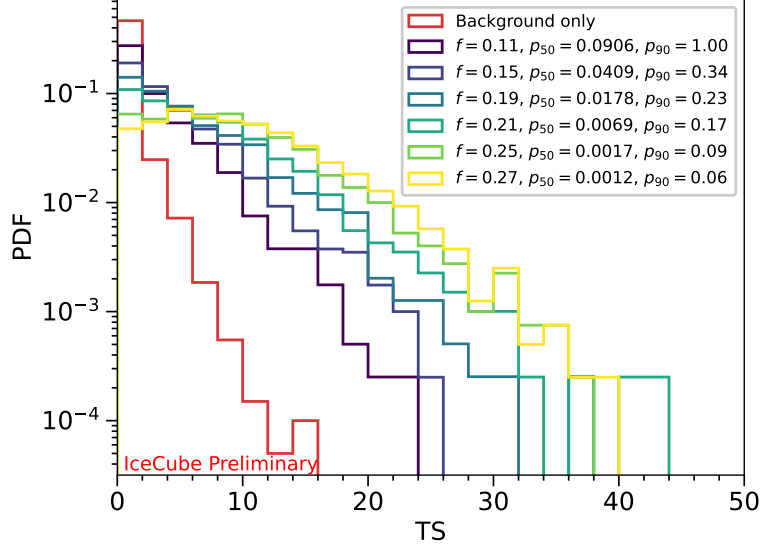


Figure 3: The TS distribution obtained for the Fermi- π^0 galactic plane template for an ensemble of pseudoexperiments at different values of f obtained following the procedure detailed in the text. As f increases TS values tend to increase as more events cluster around the galactic template. The p-values shown in the legend are obtained by comparing the 50% and 90% levels (cumulative from the right) against a background TS PDF ($f = 0$) and correspond to the probability a higher TS value would be obtained under the null.

3.1 Data-driven sensitivities to the galactic plane

Without MC, a data-driven approach was taken to estimate sensitivity to the galactic plane. The idea is to evaluate the impact of a galactic contribution as a fraction, f , of the total diffuse neutrino flux. We assume the best-fit values obtained in [5] for a single-power-law model of the diffuse astrophysical neutrino flux, and the Fermi- π^0 galactic plane spatial distribution [20, 21]. With these assumptions, each of the 164 events in data can be probabilistically categorized as atmospheric, astrophysical diffuse, or galactic thus allowing for generation of pseudoexperiments.

The procedure is as follows. The atmospheric probability is dependent on reconstructed energy and zenith using the background distributions from [5]. If an event is not categorized as atmospheric, the probability of it being of galactic origin is determined by f . For events that are categorized as galactic, a random unit vector, $\hat{\mathbf{u}}$, is sampled from its directional PDF and a second unit vector, $\hat{\mathbf{v}}$, is sampled from the Fermi- π^0 skymap within a $\pm 10^\circ$ declination band of $\hat{\mathbf{u}}$. The entire PDF is then rotated such that $\hat{\mathbf{u}}$ aligns with $\hat{\mathbf{v}}$, thus simulating that event as being of galactic origin. The entire procedure is repeated 2000 times for values of f ranging from 0.01 to 0.9, and for each ensemble of pseudoexperiments that correspond to a particular value of f a test statistic (TS) distribution can be obtained and compared to that assuming an isotropic flux (Fig. 3). Implicit are assumptions that the reconstructed distributions from [5] approximate DirectFit reconstructed quantities, and that the galactic flux follows the same spectral shape as the diffuse astrophysical flux.

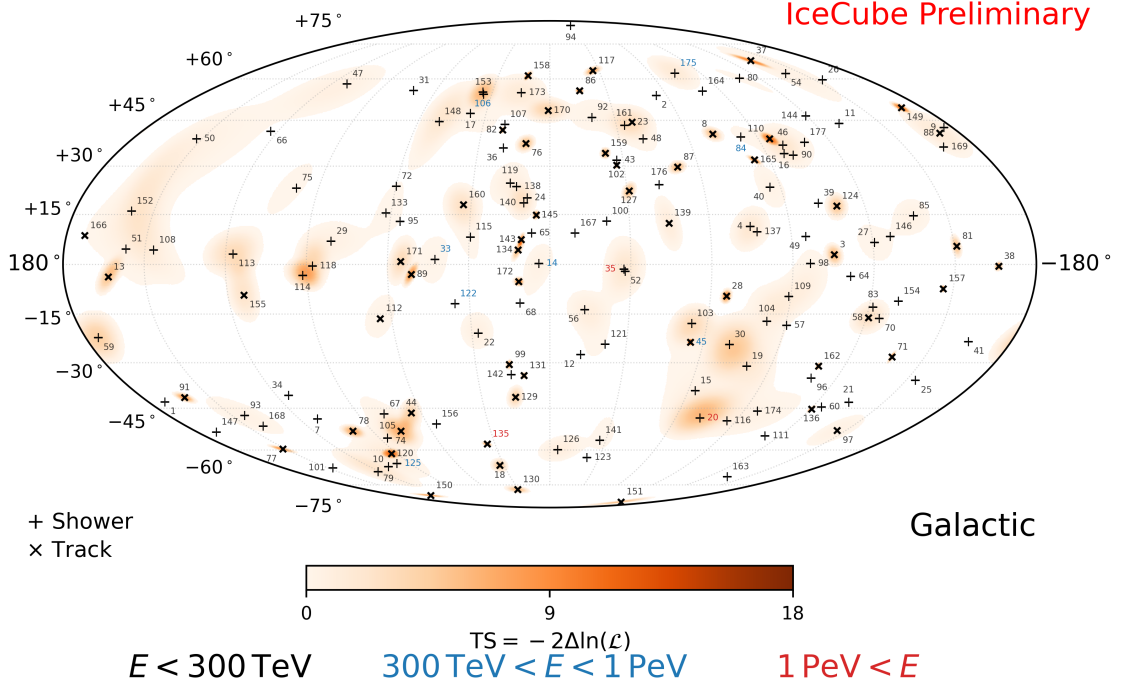


Figure 4: The TS as evaluated at points across a HEALPix map with $n_{\text{side}}=512$ [22] is indicated by the color scale. Events that were reconstructed with the shower (track) algorithm are indicated with + (x). They are also indicated by their event IDs in the skymap, which are color coded according to their reconstructed visible energy.

3.2 Results

The all sky TS map is shown in Fig. 4 in galactic coordinates. Due to the limited statistics of the sample, we do not expect to observe significant emission from point sources after trials correction. After accounting for trials, a p-value of $p = 0.17$ is obtained, consistent with existing results.

In addition to the all-sky analysis, two galactic plane clustering tests were performed. The first searched for galactic clustering within a band across the galactic plane, $|b|_{\text{max}}$, where b denotes the galactic latitude. The result is shown in Fig. 5 (blue points) for the different widths that were tested, with the most significant p-value at $|b|_{\text{max}} = 7.5^\circ$ at $p = 0.02(0.067)$ pre-trial (post-trial) with $\hat{n}_s = 13.4$. The grey lines show the pre-trial p-values obtained for 10 pseudoexperiments under the background-only hypothesis.

The second galactic plane clustering test assumed neutrino flux expectations from the Fermi- π^0 model. We find a significance of $p = 0.065$ with $\hat{n}_s = 13.8$. Based on the sensitivity studies discussed in Sec. 3.1, this is consistent with the measurement reported in [23] where the galactic contribution to the total diffuse flux is on the order of 10 percent. Based on the measured significance, an upper limit on the galactic contribution is obtained at the 90% confidence level to be $f_{90} < 27\%$ of the total diffuse neutrino flux [5].

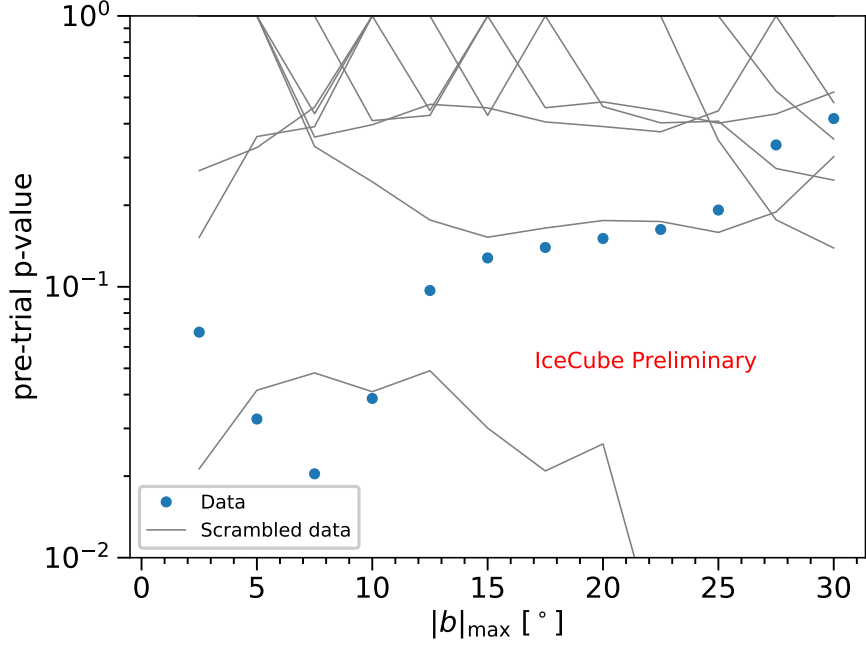


Figure 5: Pre-trial p-values obtained for data (blue points) at the $|b|_{\max}$ values indicated describing the width of a box template across the galactic plane. The same is shown for 10 pseudoexperiments under the background-only hypothesis (gray lines).

4. Conclusion

An update to the IceCube HESE dataset is provided corresponding to 12 years of data-taking. An additional 62 events were selected, on top of the existing 102 events previously reported [5]. Recent updates to ice modeling [7, 8] are taken into account by reconstructing all events with DirectFit, which fully simulates Cherenkov photon propagation through the ice [6]. For each event, the appropriate reconstruction routine (track or shower) is predetermined based on the likelihood difference under the two hypotheses. With changes in the ice model and some reclassification, shifts in direction can be expected for some events when compared to [5] (Appendix J). The full, updated dataset can be accessed at [11].

The highest energy event was reconstructed as a track to have a visible energy of 4.8 PeV. Assuming the track is due to a high-energy muon, and taking into account energy losses along the track while assuming a uniform sampling of initial muon energies [18], a preliminary estimate for the total energy of this event is (13 ± 5) PeV.

Spatial clustering tests performed include an all sky scan and two tests for emission from the galactic plane. The most significant result after trials correction is obtained for the Fermi- π^0 template at a p-value of 6.5%. Using a data-driven approach, this corresponds to a 90% upper limit of $f_{90} < 27\%$ galactic contribution to the total astrophysical neutrino flux given in [5].

References

- [1] **IceCube** Collaboration, M. G. Aartsen *et al.* *Phys. Rev. Lett.* **111** (2013) 021103.
- [2] **IceCube** Collaboration, M. G. Aartsen *et al.* *Science* **342** (2013) 1242856.
- [3] **IceCube** Collaboration, C. Kopper, W. Giang, and N. Kurahashi *PoS ICRC2015* (2016) 1081.
- [4] **IceCube** Collaboration, C. Kopper *PoS ICRC2017* (2018) 981.
- [5] **IceCube** Collaboration, R. Abbasi *et al.* *Phys. Rev. D* **104** (2021) 022002.
- [6] **IceCube** Collaboration, D. Chirkin, “Event reconstruction in IceCube based on direct event re-simulation,” in *33rd International Cosmic Ray Conference*, p. 0581. 2013.
- [7] **IceCube** Collaboration, R. Abbasi *et al.* *The Cryosphere Discussions* **2022** (2022) 1–48.
- [8] **IceCube** Collaboration, D. Chirkin and M. Rongen *PoS ICRC2023* (these proceedings) 975.
- [9] J. T. Kent *J. Roy. Statist. Soc. Ser. B* **44** no. 1, (1982) 71–80.
- [10] T. Yuan *Comput. Stat.* **36** (Mar, 2021) 409–420.
- [11] **IceCube** Collaboration, “IceCube HESE 12-year data release,” 2023. <https://doi.org/10.7910/DVN/PZNO2T>.
- [12] **IceCube** Collaboration, V. Basu and A. Balagopal V. *PoS ICRC2023* (these proceedings) 1007.
- [13] **IceCube** Collaboration, M. Silva *PoS ICRC2023* (these proceedings) 1008.
- [14] **IceCube** Collaboration, R. Naab, E. Ganster, and Z. Zhang *PoS ICRC2023* (these proceedings) 1064.
- [15] **IceCube** Collaboration, M. G. Aartsen *et al.* *JINST* **9** (2014) P03009.
- [16] **IceCube** Collaboration, T. Yuan *Nucl. Instrum. Meth. A* (2023) 168440.
- [17] **IceCube** Collaboration, T. Yuan *PoS ICRC2023* (these proceedings) 1005.
- [18] D. Chirkin and W. Rhode, “Muon Monte Carlo: A High-precision tool for muon propagation through matter,” 7, 2004.
- [19] J. Braun, J. Dumm, F. De Palma, C. Finley, A. Karle, and T. Montaruli *Astropart. Phys.* **29** (2008) 299–305.
- [20] M. Ackermann *et al.* *The Astrophysical Journal* **750** no. 1, (Apr, 2012) 3.
- [21] D. Gaggero, D. Grasso, A. Marinelli, A. Urbano, and M. Valli *The Astrophysical Journal Letters* **815** no. 2, (Dec, 2015) L25.
- [22] K. M. Górski, E. Hivon, A. J. Banday, B. D. Wandelt, F. K. Hansen, M. Reinecke, and M. Bartelman *Astrophys. J.* **622** (2005) 759–771.
- [23] **IceCube** Collaboration, R. Abbasi *et al.* *Science* **380** no. 6652, (2023) 1338–1343.

Full Author List: IceCube Collaboration

R. Abbasi¹⁷, M. Ackermann⁶³, J. Adams¹⁸, S. K. Agarwalla^{40, 64}, J. A. Aguilar¹², M. Ahlers²², J.M. Alameddine²³, N. M. Amin⁴⁴, K. Andeen⁴², G. Anton²⁶, C. Argüelles¹⁴, Y. Ashida⁵³, S. Athanasiadou⁶³, S. N. Axani⁴⁴, X. Bai⁵⁰, A. Balagopal V.⁴⁰, M. Baricevic⁴⁰, S. W. Barwick³⁰, V. Basu⁴⁰, R. Bay⁸, J. J. Beatty^{20, 21}, J. Becker Tjus^{11, 65}, J. Beise⁶¹, C. Bellenghi²⁷, C. Benning¹, S. BenZvi⁵², D. Berley¹⁹, E. Bernardini⁴⁸, D. Z. Besson³⁶, E. Blaufuss¹⁹, S. Blot⁶³, F. Bontempo³¹, J. Y. Book¹⁴, C. Boscolo Meneguolo⁴⁸, S. Böser⁴¹, O. Botner⁶¹, J. Böttcher¹, E. Bourbeau²², J. Braun⁴⁰, B. Brinson⁶, J. Brostean-Kaiser⁶³, R. T. Burley², R. S. Busse⁴³, D. Butterfield⁴⁰, M. A. Campana⁴⁹, K. Carloni¹⁴, E. G. Carnie-Bronca², S. Chattopadhyay^{40, 64}, N. Chau¹², C. Chen⁶, Z. Chen⁵⁵, D. Chirkin⁴⁰, S. Choi⁵⁶, B. A. Clark¹⁹, L. Classen⁴³, A. Coleman⁶¹, G. H. Collin¹⁵, A. Connolly^{20, 21}, J. M. Conrad¹⁵, P. Coppin¹³, P. Correa¹³, D. F. Cowen^{59, 60}, P. Dave⁶, C. De Clercq¹³, J. J. DeLaunay⁵⁸, D. Delgado¹⁴, S. Deng¹, K. Deoskar⁵⁴, A. Desai⁴⁰, P. Desati⁴⁰, K. D. de Vries¹³, G. de Wasseige³⁷, T. DeYoung²⁴, A. Diaz¹⁵, J. C. Díaz-Vélez⁴⁰, M. Dittmer⁴³, A. Domi²⁶, H. Dujmovic⁴⁰, M. A. DuVernois⁴⁰, T. Ehrhardt⁴¹, P. Eller²⁷, E. Ellinger⁶², S. El Mentawi¹, D. Elsässer²³, R. Engel^{31, 32}, H. Erpenbeck⁴⁰, J. Evans¹⁹, P. A. Evenson⁴⁴, K. L. Fan¹⁹, K. Fang⁴⁰, K. Farrag¹⁶, A. R. Fazley⁷, A. Fedynitch⁵⁷, N. Feigl¹⁰, S. Fiedlschuster²⁶, C. Finley⁵⁴, L. Fischer⁴⁰, D. Fox⁵⁹, A. Frankowiak¹¹, A. Fritz⁴¹, P. Fürst¹, J. Gallagher³⁹, E. Ganster¹, A. Garcia¹⁴, L. Gerhardt⁹, A. Ghadimi⁵⁸, C. Glaser⁶¹, T. Glauch²⁷, T. Glusenkamp^{26, 61}, N. Goehke³², J. G. Gonzalez⁴⁴, S. Goswami⁵⁸, D. Grant²⁴, S. J. Gray¹⁹, O. Gries¹, S. Griffin⁴⁰, S. Griswold⁵², K. M. Groth²², C. Günther¹, P. Gutjahr²³, C. Haack²⁶, A. Hallgren⁶¹, R. Halliday²⁴, L. Halve¹, F. Halzen⁴⁰, H. Hamdaoui⁵⁵, M. Ha Minh²⁷, K. Hanson⁴⁰, J. Hardin¹⁵, A. A. Harnisch²⁴, P. Hatch³³, A. Haungs³¹, K. Helbing⁶², J. Hellrung¹¹, F. Henningsen²⁷, L. Heuermann¹, N. Heyer⁶¹, S. Hickford⁶², A. Hidvegi⁵⁴, C. Hill¹⁶, G. C. Hill², K. D. Hoffman¹⁹, S. Hori⁴⁰, K. Hoshina^{40, 66}, W. Hou³¹, T. Huber³¹, K. Hultqvist⁵⁴, M. Hünnefeld²³, R. Hussain⁴⁰, K. Hymon²³, S. In⁵⁶, A. Ishihara¹⁶, M. Jacquart⁴⁰, O. Janik¹, M. Jansson⁵⁴, G. S. Japaridze⁵, M. Jeong⁵⁶, M. Jin¹⁴, B. J. P. Jones⁴, D. Kang³¹, W. Kang⁵⁶, X. Kang⁴⁹, A. Kappes⁴³, D. Kappesser⁴¹, L. Kardum²³, T. Karg⁶³, M. Karle²⁷, A. Karle⁴⁰, U. Katz²⁶, M. Kauer⁴⁰, J. L. Kelley⁴⁰, A. Khatee Zathul⁴⁰, A. Kheirandish^{34, 35}, J. Kiryluk⁵⁵, S. R. Klein^{8, 9}, A. Kochocki²⁴, R. Koirala⁴⁴, H. Kolanoski¹⁰, T. Kontrimas²⁷, L. Köpke⁴¹, C. Kopper²⁶, D. J. Koskinen²², P. Koundal³¹, M. Kovacevich⁴⁹, M. Kowalski^{10, 63}, T. Kozynets²², J. Krishnamoorthi^{40, 64}, K. Kruiswijk³⁷, E. Krupczak²⁴, A. Kumar⁶³, E. Kun¹¹, N. Kurahashi⁴⁹, N. Lad⁶³, C. Lagunas Gualda⁶³, M. Lamoureux³⁷, M. J. Larson¹⁹, S. Latseva¹, F. Lauber⁶², J. P. Lazar^{14, 40}, J. W. Lee⁵⁶, K. Leonard DeHolton⁶⁰, A. Leszczyńska⁴⁴, M. Lincetto¹¹, Q. R. Liu⁴⁰, M. Liubarska²⁵, E. Lohfink⁴¹, C. Love⁴⁹, C. J. Lozano Mariscal⁴³, L. Lu⁴⁰, F. Lucarelli²⁸, W. Luszczyk^{20, 21}, Y. Lyu^{8, 9}, J. Madsen⁴⁰, K. B. M. Mahn²⁴, Y. Makino⁴⁰, E. Manao²⁷, S. Mancina^{40, 48}, W. Marie Sainte⁴⁰, I. C. Mariş¹², S. Marka⁴⁶, Z. Marka⁴⁶, M. Marsee⁵⁸, I. Martinez-Soler¹⁴, R. Maruyama⁴⁵, F. Mayhew²⁴, T. McElroy²⁵, F. McNally³⁸, J. V. Mead²², K. Meagher⁴⁰, S. Mechbal⁶³, A. Medina²¹, M. Meier¹⁶, Y. Merckx¹³, L. Merten¹¹, J. Micallef²⁴, J. Mitchell⁷, T. Montaruli²⁸, R. W. Moore²⁵, Y. Morii¹⁶, R. Morse⁴⁰, M. Moulai⁴⁰, T. Mukherjee³¹, R. Naab⁶³, R. Nagai¹⁶, M. Nakos⁴⁰, U. Naumann⁶², J. Necker⁶³, A. Negi⁴, M. Neumann⁴³, H. Niederhausen²⁴, M. U. Nisa²⁴, A. Noell¹, A. Novikov⁴⁴, S. C. Nowicki²⁴, A. Obertacke Pollmann¹⁶, V. O'Dell⁴⁰, M. Oehler³¹, B. Oeyen²⁹, A. Olivas¹⁹, R. Ørsøe²⁷, J. Osborn⁴⁰, E. O'Sullivan⁶¹, H. Pandya⁴⁴, N. Park³³, G. K. Parker⁴, E. N. Paudel⁴⁴, L. Paul^{42, 50}, C. Pérez de los Heros⁶¹, J. Peterson⁴⁰, S. Philippen¹, A. Pizzuto⁴⁰, M. Plum⁵⁰, A. Pontén⁶¹, Y. Popovych⁴¹, M. Prado Rodriguez⁴⁰, B. Pries²⁴, R. Procter-Murphy¹⁹, G. T. Przybylski⁹, C. Raab³⁷, J. Rack-Helleis⁴¹, K. Rawlins³, Z. Rechav⁴⁰, A. Rehman⁴⁴, P. Reichherzer¹¹, G. Renzi¹², E. Resconi²⁷, S. Reusch⁶³, W. Rhode²³, B. Riedel⁴⁰, A. Rifaie¹, E. J. Roberts², S. Robertson^{8, 9}, S. Rodan⁵⁶, G. Roellinghoff⁵⁶, M. Rongen²⁶, C. Rott^{53, 56}, T. Ruhe²³, L. Ruohan²⁷, D. Ryckbosch²⁹, I. Safa^{14, 40}, J. Saffer³², D. Salazar-Gallegos²⁴, P. Sampathkumar³¹, S. E. Sanchez Herrera²⁴, A. Sandrock⁶², M. Santander⁵⁸, S. Sarkar²⁵, S. Sarkar⁴⁷, J. Savelberg¹, P. Savina⁴⁰, M. Schaufel¹, H. Schieler³¹, S. Schindler²⁶, L. Schlickmann¹, B. Schlüter⁴³, F. Schlüter¹², N. Schmeisser⁶², T. Schmidt¹⁹, J. Schneider²⁶, F. G. Schröder^{31, 44}, L. Schumacher²⁶, G. Schwefer¹, S. Sclafani¹⁹, D. Seckel⁴⁴, M. Seikh³⁶, S. Seunarine⁵¹, R. Shah⁴⁹, A. Sharma⁶¹, S. Shefali³², N. Shimizu¹⁶, M. Silva⁴⁰, B. Skrzypek¹⁴, B. Smithers⁴, R. Snihur⁴⁰, J. Soedingrekso²³, A. Sogaard²², D. Soldin³², P. Soldin¹, G. Sommani¹¹, C. Spannfellner²⁷, G. M. Spiczak⁵¹, C. Spiering⁶³, M. Stamatikos²¹, T. Stanev⁴⁴, T. Stetzelberger⁹, T. Stürwald⁶², T. Stuttard²², G. W. Sullivan¹⁹, I. Taboada⁶, S. Ter-Antonyan⁷, M. Thiesmeyer¹, W. G. Thompson¹⁴, J. Thwaites⁴⁰, S. Tilav⁴⁴, K. Tollefson²⁴, C. Tönnis⁵⁶, S. Toscano¹², D. Tosi⁴⁰, A. Trettin⁶³, C. F. Tung⁶, R. Turcotte³¹, J. P. Twagirayezu²⁴, B. Ty⁴⁰, M. A. Unland Elorrieta⁴³, A. K. Upadhyay^{40, 64}, K. Uphaw⁷, N. Valtonen-Mattila⁶¹, J. Vandenbroucke⁴⁰, N. van Eijndhoven¹³, D. Vannerom¹⁵, J. van Santen⁶³, J. Vara⁴³, J. Veitch-Michaelis⁴⁰, M. Venugopal³¹, M. Vereecken³⁷, S. Verpoest⁴⁴, D. Veske⁴⁶, A. Vijai¹⁹, C. Walck⁵⁴, C. Weaver²⁴, P. Weigel¹⁵, A. Weindl³¹, J. Weldert⁶⁰, C. Wendt⁴⁰, J. Werthebach²³, M. Weyrauch³¹, N. Whitehorn²⁴, C. H. Wiebusch¹, N. Willey²⁴, D. R. Williams⁵⁸, L. Witthaus²³, A. Wolf¹, M. Wolf²⁷, G. Wrede²⁶, X. W. Xu⁷, J. P. Yanez²⁵, E. Yildizci⁴⁰, S. Yoshida¹⁶, R. Young³⁶, F. Yu¹⁴, S. Yu²⁴, T. Yuan⁴⁰, Z. Zhang⁵⁵, P. Zhelnin¹⁴, M. Zimmerman⁴⁰

¹ III. Physikalisches Institut, RWTH Aachen University, D-52056 Aachen, Germany

² Department of Physics, University of Adelaide, Adelaide, 5005, Australia

³ Dept. of Physics and Astronomy, University of Alaska Anchorage, 3211 Providence Dr., Anchorage, AK 99508, USA

⁴ Dept. of Physics, University of Texas at Arlington, 502 Yates St., Science Hall Rm 108, Box 19059, Arlington, TX 76019, USA

⁵ CTSPS, Clark-Atlanta University, Atlanta, GA 30314, USA

⁶ School of Physics and Center for Relativistic Astrophysics, Georgia Institute of Technology, Atlanta, GA 30332, USA

⁷ Dept. of Physics, Southern University, Baton Rouge, LA 70813, USA

⁸ Dept. of Physics, University of California, Berkeley, CA 94720, USA

⁹ Lawrence Berkeley National Laboratory, Berkeley, CA 94720, USA

¹⁰ Institut für Physik, Humboldt-Universität zu Berlin, D-12489 Berlin, Germany

¹¹ Fakultät für Physik & Astronomie, Ruhr-Universität Bochum, D-44780 Bochum, Germany

¹² Université Libre de Bruxelles, Science Faculty CP230, B-1050 Brussels, Belgium

- ¹³ Vrije Universiteit Brussel (VUB), Dienst ELEM, B-1050 Brussels, Belgium
- ¹⁴ Department of Physics and Laboratory for Particle Physics and Cosmology, Harvard University, Cambridge, MA 02138, USA
- ¹⁵ Dept. of Physics, Massachusetts Institute of Technology, Cambridge, MA 02139, USA
- ¹⁶ Dept. of Physics and The International Center for Hadron Astrophysics, Chiba University, Chiba 263-8522, Japan
- ¹⁷ Department of Physics, Loyola University Chicago, Chicago, IL 60660, USA
- ¹⁸ Dept. of Physics and Astronomy, University of Canterbury, Private Bag 4800, Christchurch, New Zealand
- ¹⁹ Dept. of Physics, University of Maryland, College Park, MD 20742, USA
- ²⁰ Dept. of Astronomy, Ohio State University, Columbus, OH 43210, USA
- ²¹ Dept. of Physics and Center for Cosmology and Astro-Particle Physics, Ohio State University, Columbus, OH 43210, USA
- ²² Niels Bohr Institute, University of Copenhagen, DK-2100 Copenhagen, Denmark
- ²³ Dept. of Physics, TU Dortmund University, D-44221 Dortmund, Germany
- ²⁴ Dept. of Physics and Astronomy, Michigan State University, East Lansing, MI 48824, USA
- ²⁵ Dept. of Physics, University of Alberta, Edmonton, Alberta, Canada T6G 2E1
- ²⁶ Erlangen Centre for Astroparticle Physics, Friedrich-Alexander-Universität Erlangen-Nürnberg, D-91058 Erlangen, Germany
- ²⁷ Technical University of Munich, TUM School of Natural Sciences, Department of Physics, D-85748 Garching bei München, Germany
- ²⁸ Département de physique nucléaire et corpusculaire, Université de Genève, CH-1211 Genève, Switzerland
- ²⁹ Dept. of Physics and Astronomy, University of Gent, B-9000 Gent, Belgium
- ³⁰ Dept. of Physics and Astronomy, University of California, Irvine, CA 92697, USA
- ³¹ Karlsruhe Institute of Technology, Institute for Astroparticle Physics, D-76021 Karlsruhe, Germany
- ³² Karlsruhe Institute of Technology, Institute of Experimental Particle Physics, D-76021 Karlsruhe, Germany
- ³³ Dept. of Physics, Engineering Physics, and Astronomy, Queen's University, Kingston, ON K7L 3N6, Canada
- ³⁴ Department of Physics & Astronomy, University of Nevada, Las Vegas, NV, 89154, USA
- ³⁵ Nevada Center for Astrophysics, University of Nevada, Las Vegas, NV 89154, USA
- ³⁶ Dept. of Physics and Astronomy, University of Kansas, Lawrence, KS 66045, USA
- ³⁷ Centre for Cosmology, Particle Physics and Phenomenology - CP3, Université catholique de Louvain, Louvain-la-Neuve, Belgium
- ³⁸ Department of Physics, Mercer University, Macon, GA 31207-0001, USA
- ³⁹ Dept. of Astronomy, University of Wisconsin–Madison, Madison, WI 53706, USA
- ⁴⁰ Dept. of Physics and Wisconsin IceCube Particle Astrophysics Center, University of Wisconsin–Madison, Madison, WI 53706, USA
- ⁴¹ Institute of Physics, University of Mainz, Staudinger Weg 7, D-55099 Mainz, Germany
- ⁴² Department of Physics, Marquette University, Milwaukee, WI, 53201, USA
- ⁴³ Institut für Kernphysik, Westfälische Wilhelms-Universität Münster, D-48149 Münster, Germany
- ⁴⁴ Bartol Research Institute and Dept. of Physics and Astronomy, University of Delaware, Newark, DE 19716, USA
- ⁴⁵ Dept. of Physics, Yale University, New Haven, CT 06520, USA
- ⁴⁶ Columbia Astrophysics and Nevis Laboratories, Columbia University, New York, NY 10027, USA
- ⁴⁷ Dept. of Physics, University of Oxford, Parks Road, Oxford OX1 3PU, United Kingdom
- ⁴⁸ Dipartimento di Fisica e Astronomia Galileo Galilei, Università Degli Studi di Padova, 35122 Padova PD, Italy
- ⁴⁹ Dept. of Physics, Drexel University, 3141 Chestnut Street, Philadelphia, PA 19104, USA
- ⁵⁰ Physics Department, South Dakota School of Mines and Technology, Rapid City, SD 57701, USA
- ⁵¹ Dept. of Physics, University of Wisconsin, River Falls, WI 54022, USA
- ⁵² Dept. of Physics and Astronomy, University of Rochester, Rochester, NY 14627, USA
- ⁵³ Department of Physics and Astronomy, University of Utah, Salt Lake City, UT 84112, USA
- ⁵⁴ Oskar Klein Centre and Dept. of Physics, Stockholm University, SE-10691 Stockholm, Sweden
- ⁵⁵ Dept. of Physics and Astronomy, Stony Brook University, Stony Brook, NY 11794-3800, USA
- ⁵⁶ Dept. of Physics, Sungkyunkwan University, Suwon 16419, Korea
- ⁵⁷ Institute of Physics, Academia Sinica, Taipei, 11529, Taiwan
- ⁵⁸ Dept. of Physics and Astronomy, University of Alabama, Tuscaloosa, AL 35487, USA
- ⁵⁹ Dept. of Astronomy and Astrophysics, Pennsylvania State University, University Park, PA 16802, USA
- ⁶⁰ Dept. of Physics, Pennsylvania State University, University Park, PA 16802, USA
- ⁶¹ Dept. of Physics and Astronomy, Uppsala University, Box 516, S-75120 Uppsala, Sweden
- ⁶² Dept. of Physics, University of Wuppertal, D-42119 Wuppertal, Germany
- ⁶³ Deutsches Elektronen-Synchrotron DESY, Platanenallee 6, 15738 Zeuthen, Germany
- ⁶⁴ Institute of Physics, Sachivalaya Marg, Sainik School Post, Bhubaneswar 751005, India
- ⁶⁵ Department of Space, Earth and Environment, Chalmers University of Technology, 412 96 Gothenburg, Sweden
- ⁶⁶ Earthquake Research Institute, University of Tokyo, Bunkyo, Tokyo 113-0032, Japan

Acknowledgements

The authors gratefully acknowledge the support from the following agencies and institutions: USA – U.S. National Science Foundation-Office of Polar Programs, U.S. National Science Foundation-Physics Division, U.S. National Science Foundation-EPSCoR, Wisconsin Alumni Research Foundation, Center for High Throughput Computing (CHTC) at the University of Wisconsin–Madison, Open Science

Grid (OSG), Advanced Cyberinfrastructure Coordination Ecosystem: Services & Support (ACCESS), Frontera computing project at the Texas Advanced Computing Center, U.S. Department of Energy-National Energy Research Scientific Computing Center, Particle astrophysics research computing center at the University of Maryland, Institute for Cyber-Enabled Research at Michigan State University, and Astroparticle physics computational facility at Marquette University; Belgium – Funds for Scientific Research (FRS-FNRS and FWO), FWO Odysseus and Big Science programmes, and Belgian Federal Science Policy Office (Belspo); Germany – Bundesministerium für Bildung und Forschung (BMBF), Deutsche Forschungsgemeinschaft (DFG), Helmholtz Alliance for Astroparticle Physics (HAP), Initiative and Networking Fund of the Helmholtz Association, Deutsches Elektronen Synchrotron (DESY), and High Performance Computing cluster of the RWTH Aachen; Sweden – Swedish Research Council, Swedish Polar Research Secretariat, Swedish National Infrastructure for Computing (SNIC), and Knut and Alice Wallenberg Foundation; European Union – EGI Advanced Computing for research; Australia – Australian Research Council; Canada – Natural Sciences and Engineering Research Council of Canada, Calcul Québec, Compute Ontario, Canada Foundation for Innovation, WestGrid, and Compute Canada; Denmark – Villum Fonden, Carlsberg Foundation, and European Commission; New Zealand – Marsden Fund; Japan – Japan Society for Promotion of Science (JSPS) and Institute for Global Prominent Research (IGPR) of Chiba University; Korea – National Research Foundation of Korea (NRF); Switzerland – Swiss National Science Foundation (SNSF); United Kingdom – Department of Physics, University of Oxford.